







Phonon-exciton Interactions in WSe_2 under a quantizing magnetic field

Zhipeng Li^{1,10}, Tianmeng Wang ^{1,10}, Shengnan Miao^{1,10}, Yunmei Li^{2,10}, Zhenguang Lu^{3,4}, Chenhao Jin ⁵, Zhen Lian¹, Yuze Meng¹, Mark Blei⁶, Takashi Taniguchi⁷, Kenji Watanabe ⁷, Sefaattin Tongay⁶, Wang Yao ⁸, Dmitry Smirnov ³, Chuanwei Zhang² & Su-Fei Shi ^{1,9}✉

Strong many-body interaction in two-dimensional transitional metal dichalcogenides provides a unique platform to study the interplay between different quasiparticles, such as prominent phonon replica emission and modified valley-selection rules. A large out-of-plane magnetic field is expected to modify the exciton-phonon interactions by quantizing excitons into discrete Landau levels, which is largely unexplored. Here, we observe the Landau levels originating from phonon-exciton complexes and directly probe exciton-phonon interaction under a quantizing magnetic field. Phonon-exciton interaction lifts the inter-Landau-level transition selection rules for dark trions, manifested by a distinctively different Landau fan pattern compared to bright trions. This allows us to experimentally extract the effective mass of both holes and electrons. The onset of Landau quantization coincides with a significant increase of the valley-Zeeman shift, suggesting strong many-body effects on the phonon-exciton interaction. Our work demonstrates monolayer WSe_2 as an intriguing playground to study phonon-exciton interactions and their interplay with charge, spin, and valley.

¹Department of Chemical and Biological Engineering, Rensselaer Polytechnic Institute, Troy, NY 12180, USA. ²Department of Physics, The University of Texas at Dallas, Richardson, TX 75080, USA. ³National High Magnetic Field Lab, Tallahassee, FL 32310, USA. ⁴Department of Physics, Florida State University, Tallahassee, FL 32306, USA. ⁵Kavli Institute, Cornell University, Ithaca, NY 14853, USA. ⁶School for Engineering of Matter, Transport and Energy, Arizona State University, Tempe, AZ 85287, USA. ⁷National Institute for Materials Science, 1-1 Namiki, Tsukuba 305-0044, Japan. ⁸Department of Physics, University of Hong Kong, Hong Kong, China. ⁹Department of Electrical, Computer & Systems Engineering, Rensselaer Polytechnic Institute, Troy, NY 12180, USA. ¹⁰These authors contributed equally: Zhipeng Li, Tianmeng Wang, Shengnan Miao, Yunmei Li. ✉email: shis2@rpi.edu

Phonons, quasiparticles describing the collective vibrations of lattice, can strongly interact with excitons in semiconductor nanostructures^{1–9} and significantly influence the light emission and energy relaxation^{2–4}. The strong Coulomb interaction and many-body effects in monolayer transition metal dichalcogenides (TMDCs)^{10–13} significantly enhance the phonon–exciton interaction, which was shown to reveal the silent Raman modes in boron nitride (BN) encapsulated monolayer WSe₂^{9,14}. The valley degree of freedom of the excitonic complexes also leads to types of phonon–exciton interactions that brighten the spin-forbidden dark exciton and intervalley exciton in WSe₂ through chiral phonon modes at Γ point⁵ and K point¹, respectively, resulting in phonon replica PL with long lifetime and large valley polarization. Due to the valley–spin locking^{15,16} and the nontrivial Berry phase^{17–19}, the phonon–exciton interaction can be even more intriguing with the application of a large out-of-plane magnetic field, which induces valley-polarized Landau levels (LLs) and dictates the unique selection rules of the inter-LL transition^{20–22}.

In this work, we explore the phonon–exciton interaction in the regime of Landau quantization. We achieve this through PL spectroscopy of a high-quality monolayer WSe₂ device, which clearly resolves PL peaks from different phonon replicas, especially the phonon replica of the dark trions. We found that K phonons can lift the inter-LL transition selection rules of positive dark trions, resulting in the distinctively different Landau fan in the PL spectra compared with that from the bright trion. Exploiting the unique phonon–exciton interaction in WSe₂, we can directly probe the hole LL in the valence band, bypassing the limitations of most optical spectroscopy techniques that can only probe the Landau quantization of combined electron–hole pairs. The simultaneous observation of the Landau quantization of the dark trion phonon replica and the bright trion also allows us to experimentally extract the electron and hole masses separately, which exhibit surprisingly large asymmetry, in stark contrast to common assumptions^{23–25}. Interestingly, the onset of the phonon replica PL quantization also correlates with a drastic change of valley-Zeeman shift characterized by an increase of Landé g-factor from 5.5 to 18.0, suggesting strong many-body interactions.

Results

Phonon replicas of excitonic particles in monolayer WSe₂. The BN encapsulated monolayer WSe₂ device was fabricated through a pickup method similar to previous reports^{5,13,26}. The device structure is schematically shown in Fig. 1a, and a typical optical microscope image of the device is shown in Fig. 1b. We investigate the helicity-resolved PL spectra of the monolayer WSe₂ as a function of the gate voltage at 4.2 K. The gate-voltage-dependent PL spectra in $\sigma^- \sigma^-$ (σ^- excitation and σ^- detection) and $\sigma^- \sigma^+$ (σ^- excitation and σ^+ detection) configurations, shown in Fig. 1c, d, exhibit high spectral quality and a series of well-resolved PL peaks arising from various excitonic complexes. A significant number of the excitonic complexes have been identified previously, including the exciton (X_0), intervalley n-trions (X_1^-), intravalley n-trions (X_2^-), dark exciton (X_D)^{27–29}, positive, and negative dark trions (X_D^+ and X_D^-)^{26,30,31}. Phonon replicas of the spin-forbidden dark exciton (X_D^R) and the momentum-dark intervalley exciton (X_1^R) have also been observed previously^{1,5}, due to the long lifetime of the dark excitonic complexes. Because of the valley degree of freedom, angular momentum conservation has to be considered in the phonon–exciton interaction in TMDCs, and the chiral phonon mode is involved in X_D^R (linear combination of two doubly degenerate $E''(\Gamma)$ or X_1^R (LO(E')/K))^{1,5}. In the charge-neutral region (gate voltage from -0.10 to 0.21 V in Fig. 1c, d), one additional PL

peak X_1^{R2} (1.6788 eV in Fig. 1d) emerges in the $\sigma^- \sigma^+$ configuration due to its negative valley polarization. The X_1^{R2} is another phonon replica of the intervalley exciton with the LA(K) phonon involved (see Supplementary Note 2 for details), consistent with a very recent report³².

Interestingly, in the highly p-doped region, the PL of the bright trion peak (X^+) exhibits a significant redshift after the gate voltage of approximately -2.5 V (Fig. 1a, b), and this gate dependence is closely followed by the dark trion (X_D^+), along with five PL peaks labeled as $X_D^{+(R_1)}$, $X_D^{+(R_2)}$, $X_D^{+(R_3)}$, $X_D^{+(R_4)}$, and $X_D^{+(R_5)}$ (Fig. 2a, b). This constant energy differences between each of the five emerging peaks and the dark trion for different gate voltages suggest that these five peaks are all phonon replicas (associated with different phonon modes) of the long-lived positive dark trion (or dark p-trion). Due to the three-particle nature of the positive dark trion, the electron–hole recombination can occur either in the same valley or across the opposite valley, assisted by Γ (Fig. 2d) or K phonons (Fig. 2c). The $X_D^{+(R_1)}$ and $X_D^{+(R_4)}$ peaks are lower than the dark trion peak by 13.1 and 26.4 meV, respectively, in good agreement with the theoretically calculated energy of the TA(K) phonon (11.6 to 11.7 meV)^{1,2,32} and LO(E')/K phonon (24.6 or 26.0 meV)^{1,32}, respectively, (see Supplementary Table 1 for details). The phonon replica nature of the $X_D^{+(R_1)}$ and $X_D^{+(R_4)}$ peaks are also confirmed later by the measured Landé g-factor, which is the same as the positive dark trion within the experimental uncertainty. The $X_D^{+(R_2)}$ and $X_D^{+(R_3)}$ peaks are ~ 17.3 and ~ 21.6 meV below the positive dark trion X_D^+ , suggesting that they are the phonon replicas involving the LA (K) phonon (calculated energy of 16.8 to 17.0 meV)^{1,2,32} and $E''(\Gamma)$ (calculated energy of 21.8 meV)⁵, respectively, also consistent with a very recent report³². It is worth noting that the phonon energy can be experimentally extracted from the phonon replicas of the positive dark trion without worrying about the exchange interaction (see Supplementary Note 3 for details). As the phonon replicas associated with $E''(\Gamma)$, LO(E')/K, and LA(K) modes are also found in the charge-neutral region, the corresponding peak of X_D^R , X_1^R , and X_1^{R2} can then be used to determine the exchange interaction, which is extracted to be 9.3–10.1 meV (see Supplementary Note 3 for details). The phonon modes associated with $X_D^{+(R_1)}$, $X_D^{+(R_2)}$, $X_D^{+(R_3)}$, and $X_D^{+(R_4)}$ are schematically shown in Fig. 2e. The corresponding phonon mode replicas can also be found for the negative dark trion (or dark n-trion) except for $X_D^{-(R_2)}$, labeled as $X_D^{-(R_1)}$, $X_D^{-(R_3)}$, and $X_D^{-(R_4)}$ (Fig. 2a, b). $X_D^{-(R_2)}$ was not observed, possibly due to the strong PL at its neighborhood from the mysterious PL peak M^- . The PL peaks of M^- , $X_D^{+(R_5)}$, $X_D^{-(R_5)}$, and $X_D^{-(R_5)}$ remain unidentified (see Supplementary Notes 5 and 7).

Landau quantization in the PL spectra. A large out-of-plane magnetic field not only lifts the valley degeneracy by lowering the valence band maximum of the K' valley compared with that of the K valley (Fig. 3e, f); it also induces the valley-polarized LLs. We optically pump the WSe₂ in the K' valley and detect PL from the K' valley ($\sigma^- \sigma^-$ configuration). In the highly p-doped WSe₂ (boxed region in Fig. 3a, b), with an out-of-plane magnetic field of 17 T, we found Landau fan like oscillations emerging in the helicity-resolved PL spectra. These oscillations can be categorized into three sets: one set of parallel strips accompanying the positive bright trion (X^+) and the other two sets accompanying the phonon replicas of the dark trion ($X_D^{+(R_1)}$ and $X_D^{+(R_4)}$) (Fig. 3b). We attribute these oscillation features to the LL formation.

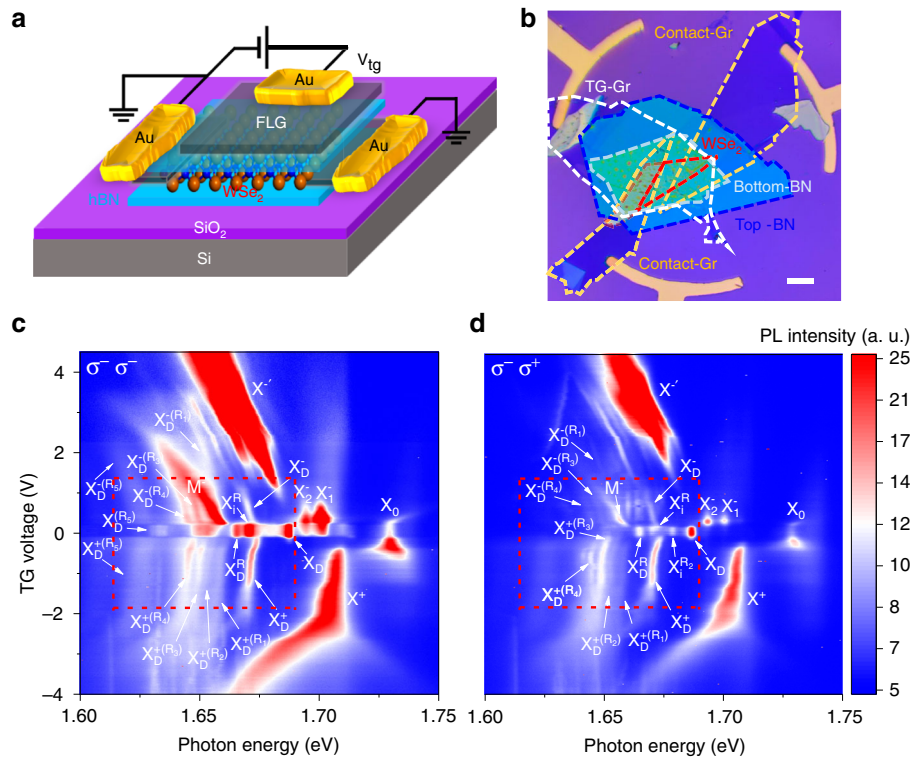


Fig. 1 PL spectra of BN encapsulated monolayer WSe₂ at 4.2 K. **a** Schematic of the h-BN encapsulated monolayer WSe₂ device. **b** Optical microscope image of the device. The flakes of few-layer h-BN, few-layer graphene, and monolayer WSe₂ are outlined with different colors. The scale bar is 20 μm. **c, d** PL spectra of the monolayer WSe₂ as a function of top gate voltage for the σ⁻σ⁻ configuration (σ⁻ excitation and σ⁻ detection) and the σ⁻σ⁺ configuration (σ⁻ excitation and σ⁺ detection), respectively, with a CW laser excitation centered at 1.879 eV and an excitation power of 50 μW. The color represents the PL intensity. Besides the bright exciton (X₀), dark exciton (X_D), positive trion (X⁺), intervalley trion (X₂⁻), intravalley trion (X₂⁺), and the recently discovered positive dark trion (X_D⁺), negative dark trion (X_D⁻), intervalley exciton-phonon replica (X_D^R), and dark exciton-phonon replica (X_D^R), there are additional emerging excitonic states that are labeled as X_D^{+(R₁)}}, X_D^{-(R₁)}}, X_D^{+(R₂)}}, X_D^{-(R₂)}}, X_D^{+(R₃)}}, X_D^{-(R₃)}}, X_D^{+(R₄)}}, X_D^{-(R₄)}}, X_D^{+(R₅)}}, and X_D^{-(R₅)}} in the electron- and hole-doping regions. In addition, X₁^{R2} emerges in the σ⁻σ⁺ configuration.

The energy spacing between the oscillations increases linearly as a function of the magnetic field strength (see Supplementary Note 5), consistent with our interpretation.

The Landau fan patterns can be seen more clearly from PL spectra at the representative gate voltage of -3 V and B field of 17 T, shown in Fig. 3c (corresponding to the horizontal dashed line in Fig. 3b). The PL from the bright trion (X⁺) shows multiple peaks with even energy spacing of ~7.0 meV (red curve in Fig. 3c). The electron-hole recombination in the K' valley is constrained by the valley-polarized selection rules in the K' valley and only the n → -(n-1) transition is allowed^{20,22}. At a given gate voltage, this gives rise to evenly spaced Landau fans with separation, which can be expressed phonematically as $\frac{\hbar B}{\mu^*}$, where μ^* is the effective reduced mass of exciton. In addition, in the highly p-doped regime, the optically excited electron is mostly at the bottom of the conduction band. Therefore, PL intensity is strongest at the lowest energy peak (associated with the 0 → -1 inter-LL transition) and decreases quickly for higher-energy transition. These behaviors match well with our experimental observation in Fig. 3c. And we show the extracted value of μ^* as a function of the gate voltage in Fig. 3d.

Surprisingly, the Landau fan pattern from dark trion phonon replica X_D^{+(R₁)}} and X_D^{+(R₄)}} shows remarkably different behaviors: First, the energy spacing of the oscillations is $\sim 3.9 \pm 0.2$ meV, about half of the value for the bright trion ($\sim 7.0 \pm 0.2$ meV). In addition, the intensity of the oscillations remains largely constant with energy for dark trion phonon replicas. These two distinctive differences suggest that the recombination processes underlying

dark trion phonon replicas have very different inter-LL transition selection rules.

In a dark trion phonon replica, the recombination of the electron and hole can either occur in the same valley (K valley here) through emitting a Γ phonon or across the valley through emitting a K phonon (Fig. 2c). We do not observe the LL quantization associated with the Γ phonon replica of the positive dark trion, likely due to the weakened coupling with the Γ phonon in the presence of the large out-of-plane field (see Supplementary Note 4). For the K phonon replica, the electron can recombine with the hole in the other valley by emitting a K phonon. From the Fermi's golden rule, the inter-LL transition rate from n in K valley to -n' in K' valley (minus sign means valence band) is given by³³

$$P_{n \rightarrow -n'} = \frac{2\pi}{\hbar} \sum_{\nu} \left| \sum_m \frac{\langle -n', -|H_{el}|m, -\rangle \langle m, -|H_{ep}|n, +\rangle}{E_{m,-} - E_{n,+} + \hbar\omega_{K\nu}} \right|^2 \delta(E_{n,+} - E_{-n',-} - \hbar\omega - \hbar\omega_{K\nu}). \tag{1}$$

where H_{ep} is the electron-phonon interaction Hamiltonian and H_{el} is the electron-light coupling Hamiltonian (see Supplementary Note 10 for details). $\hbar\omega_{K\nu}$ is the K phonon energy with mode ν . $|n, +\rangle$ ($|n, -\rangle$) represents the LL state in K (K') valley. The selection rule for optical intra-LL transition is $n' = m + 1$. Different from the optical process, the phonon scattering process $\langle m, -|H_{ep}|n, +\rangle$ is not limited by the selection rules (see Supplementary Note 10 for details). Thus, the phonon-exciton interaction involved here lifts the constraint of inter-LL transition selection rules (see Supplementary Note 10). As a result, electrons

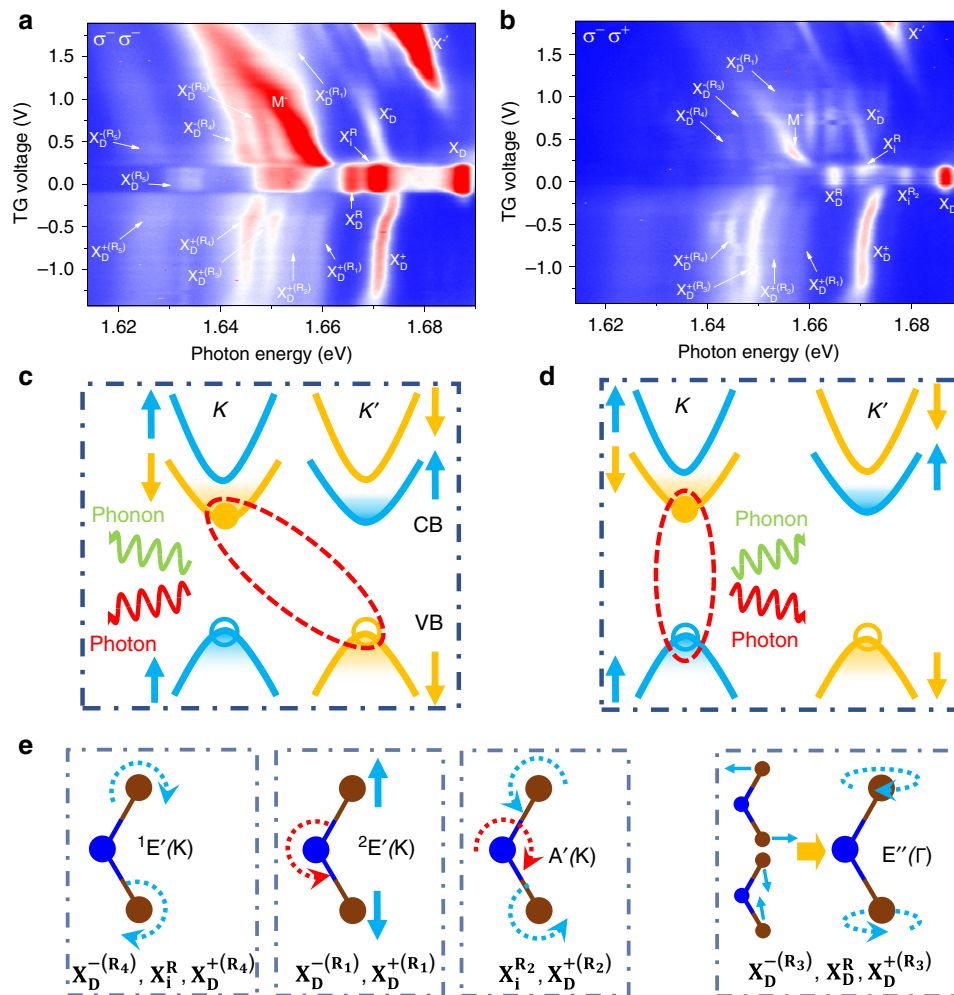


Fig. 2 Phonon replicas of the dark trions. **a, b** Zoom-in color plots of the PL spectra for the boxed region (red dashed line) in Fig. 1c, d, respectively. The color represents the PL intensity. **c, d** Schematics of light emission from the positive dark trion state through the interlayer electron-hole recombination assisted by emitting a K phonon (**c**), or through the intralayer recombination assisted by emitting a Γ phonon. **e** Illustration of different phonon modes and associated phonon replicas.

in the K valley can recombine with holes in any LLs in the K' valley, as shown in Fig. 3d. The oscillation spacing will be determined solely by the Δ_{LL}^V . In addition, the recombination probability will be similar for holes at different LLs in the valence band, as the occupation probability for holes in the first few LLs are all close to unity in the highly p-doped WSe₂. This interpretation is consistent with the aforementioned experimental observations.

Effective mass asymmetry between the electron and hole.

Through the oscillation period of phonon replica of the positive dark trion, we can experimentally determine the LL spacing of the valence band $\Delta_{LL}^V = \frac{e\hbar B}{m_h^*}$, where m_h^* is the effective hole mass and B is the magnetic field strength. For the gate voltage of -3 V, the extracted valence band LL spacing is $\sim 3.9 \pm 0.2$ meV (Fig. 3c), corresponding to $m_h^* \sim 0.50m_0$, with m_0 being the free electron mass in the vacuum. Using the experimentally extracted oscillation spacing as a function of the gate voltage (see Supplementary Note 5), we can extract the gate-voltage-dependent effective hole mass as shown in Fig. 3d. The effective mass of the hole decreases from $0.61m_0$ to $0.45m_0$ as the voltage decreases from -2.6 to -4.0 V. The value of $\sim 0.45m_0$ at the highest p-doping studied in this work (gate voltage of -4.0 V) is close to the theoretically

predicted value of $0.4m_0$, while the much-enhanced value of $0.61m_0$ indicates strong interactions at the gate voltage of -2.6 V.

At the same time, we also observe the LL quantization of the bright trion, which probes the combined Landau quantization of the exciton. Our top BN flake is ~ 9 nm thick, which corresponding to a gating efficiency of $2.15 \times 10^{12} \text{ cm}^{-2} \text{ V}^{-1}$ based on a geometry capacitance model (see Supplementary Note 9 for details). As a result, at the onset of the Landau fan of the bright trion at approximately -2.6 V, the density of hole is estimated to be $5.4 \times 10^{12} \text{ cm}^{-2}$ (onset of the p-doping at -0.1 V, Fig. 1). In this strongly p-doped regime, we expect a much reduced Coulomb interaction and assume a small exciton binding energy to help extract the effective electron mass²⁰. For the loosely bound electron-hole pair²⁰, the LL of the exciton $\frac{e\hbar B}{\mu}$ can be expressed as the summation of the LL spacing of the conduction band (Δ_{LL}^C) and valence band Δ_{LL}^V , i.e., $\Delta_{LL}^C + \Delta_{LL}^V = \frac{e\hbar B}{\mu}$. Therefore, we would have the expression $\frac{1}{\mu} = \frac{1}{m_h^*} + \frac{1}{m_e^*}$, which we can use to extract the effective electron mass of the electron, m_e^* ¹⁹. This picture is confirmed by the observation that the LL spacing from the exciton-phonon complex is always about half of the value for the bright trion for the gate voltage range we studied (Supplementary Fig. 11). Between the gate voltage -3.5 to -2.6 V, the extracted effective mass of the exciton varies from $0.25m_0$ to $0.38m_0$

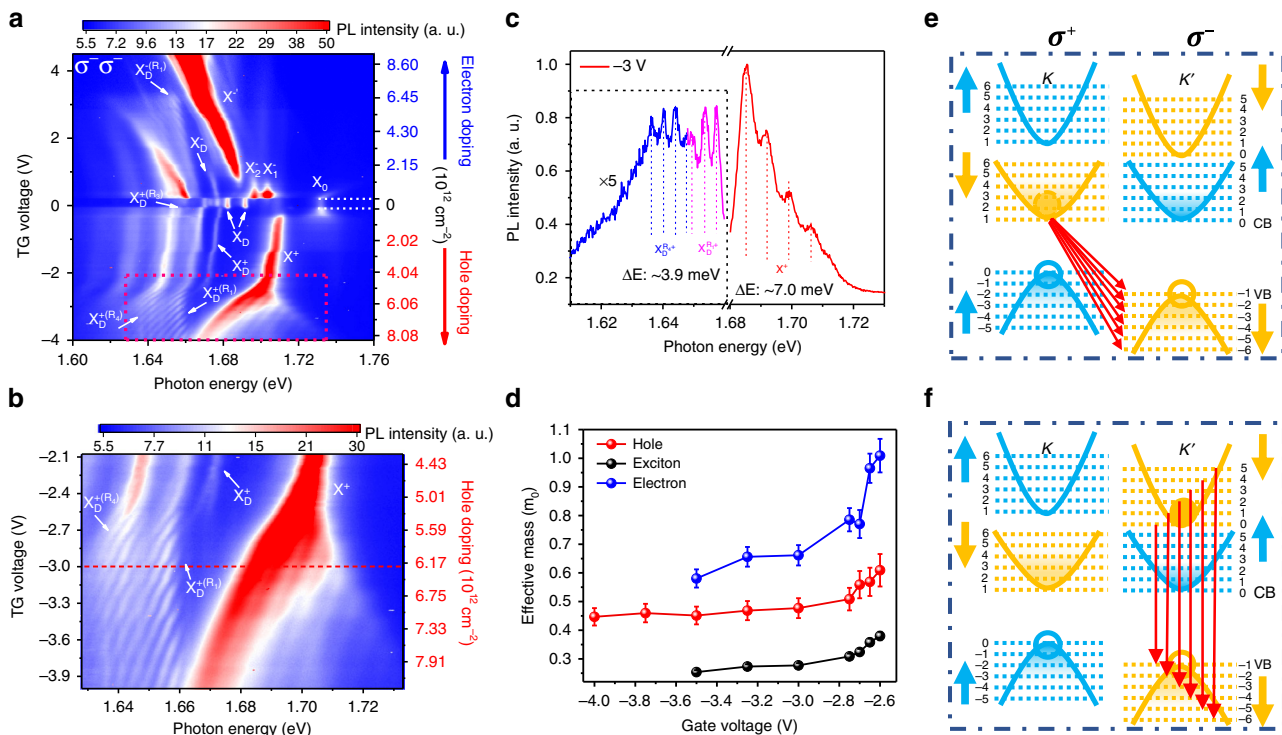


Fig. 3 Magneto-PL spectra of BN encapsulated monolayer WSe₂. **a** 2D color plot of PL spectra as a function of the top gate voltage. The X⁺, X_D^{+(R₁)}, X_D^{-(R₁)}, and X_D^{+(R₄)} peaks show clear Landau quantization. The color represents the PL intensity, and the calculated carrier density is shown in the right axis with region from -0.1 to 0.2 V being charge-neutral. **b** Zoom-in PL spectra for the boxed region in **a**. **c** The PL spectra for the gate voltage of -3 V (horizontal dashed line in **b**). The PL intensity in the energy range of X_D^{+(R₁)} and X_D^{-(R₁)} peaks (dashed box) is multiplied by five times. The oscillation spacing, ΔE, is ~3.9 meV for X_D^{+(R₁)} and X_D^{-(R₁)}, and ~7.0 meV for X⁺. **d** The effective mass of hole, electron, and exciton in the hole-doping region. The error bar indicates the standard deviation of the LL spacing determined from the PL spectra. **e, f** Schematic of the inter-band LL transitions for different excitonic states: X_D⁺, X_D^{-(R₁)} (**e**) and X⁺ (**f**).

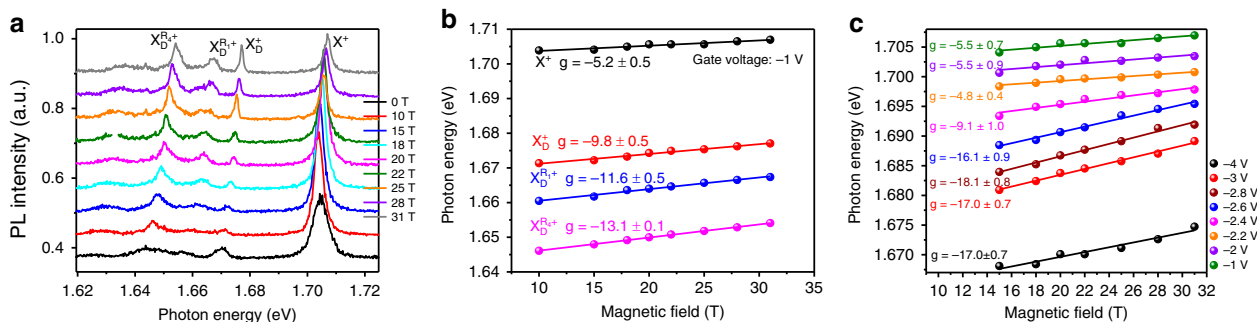


Fig. 4 Valley-Zeeman shift from the magneto-PL spectra. **a** PL spectra in the σ⁺σ⁻ configuration at the gate voltage of -1 V for various magnetic field strengths. **b** The extracted PL peak position (solid dots) of X⁺, X_D⁺, X_D^{-(R₁)}, and X_D^{+(R₄)} as a function of the magnetic field at 4.2 K for the gate voltage of -1 V. Solid lines are the linear fittings, with the extracted g-factor labeled. **c** The extracted g-factors of the bright positive trion X⁺ for different gate voltages.

(Fig. 3d), similar to what has been extracted from the absorption spectra of n-doped WSe₂²⁰. However, the associated effective electron mass is much larger than that of hole, 0.58m₀ to 1.01m₀ between the gate voltage -3.5 to -2.6 V. At the same experimental condition, this larger effective mass of electron than hole by as large as >50% (Fig. 3d), is in stark contrast to the typical assumption of electron-hole symmetry^{20,23–25}.

The electron mass can also be directly extracted for n-doped WSe₂, from the Landau quantization of the PL from the phonon replica of the negative dark trion (X_D^{-(R₁)}, see Fig. 3a and Supplementary Note 5). The effective electron mass is extracted to be ~0.8m₀ between the gate voltage of 2.25–2.85 V. This value falls in the range of the effective electron mass extracted from

the p-doped WSe₂ and is also significantly larger than the effective mass of hole.

Gate-dependent valley-Zeeman shift. Under the out-of-plane magnetic field, the PL peak of excitonic complexes from one particular valley will exhibit a linear shift due to the valley-Zeeman effect (Fig. 4a for K' valley), which can be used to determine the g-factor and thus the nature of the excitonic complexes^{1,5,13,26}. As shown in Fig. 4b, at the gate voltage of -1 V, the g-factor for the bright trion and dark positive trion is -5.2 and -9.8, respectively, consistent with the previous report^{11,26,29,34}. For the dark trion phonon replica involving K phonons, the g-factor should be determined by the recombination

of electron–hole pair from the opposite valleys, which is theoretically expected to be -12 (see Supplementary Note 6). This value agrees well with that of the dark trion replica, -11.6 for $X_D^{+(R_1)}$ and -13.1 for $X_D^{+(R_2)}$, confirming that these two PL peaks are the phonon replicas of the positive dark trion.

Interestingly, the magnitude of the g -factor of the bright trion increases significantly when the p -doping increases, with an abrupt change at the gate voltage of -2.6 V (Fig. 4c). This similar enhancement of the g -factor has been observed in the strongly n -doped WSe_2 for the plasma mode^{20,35}. This peculiar abrupt enhancement of g -factor magnitude at the gate voltage of -2.6 V also closely correlates with the significant increase of the effective mass of electron and hole, suggesting the effects of many-body interactions. In fact, it has been shown that, in the highly p -doped regime, the simple trion picture should be better described with the picture of exciton–polaron³⁶, in which the exciton interacts with all the holes in the opposite valley. Future exploration of the phonon–exciton interactions in the presence of valley-polarized LLs will strengthen our understanding of the exciting quantum many-body effects in the monolayer WSe_2 platform.

Discussion

In summary, we have shown the observation of Landau quantization of exciton–phonon complexes in monolayer WSe_2 under a large out-of-plane magnetic field. Although optical spectroscopy has proven to be a powerful tool to study Landau quantization in two-dimension^{37–39}, the two-particle nature makes it challenging to directly probe the electron or hole mass, and we cannot directly compare the obtained information from the optical spectroscopy with the single-particle information extracted from the low-temperature transport measurements. Here, taking advantage of the unique phonon–exciton interactions in WSe_2 , we bridge these two worlds through the sensitive PL spectroscopy, whose non-coherent nature helps reveal the single-particle information. The obtained electron mass and hole mass exhibit unexpected asymmetry, likely arising from many-body effects and will inspire future theoretical investigation. The advancement will be crucial for the understanding of mobility and thus the application of TMDCs-based devices. Further, the unique interaction between phonons and dark excitons in the presence of the valley-polarized LLs may shed light on potential avenues of manipulating spin and valley for valleytronics spintronics.

Method

Device fabrication. The BN encapsulated WSe_2 device was fabricated through a pickup dry transfer method^{5,13,26}. Monolayer WSe_2 , few-layer graphene, and few-layer BN were exfoliated onto 300 nm SiO_2/Si substrate and identified with an optical microscope by the optical contrast. The few-layer BN flake, monolayer WSe_2 , two few-layer graphenes, and another few-layer BN flake were picked up by a PET stamp sequentially. The prepared stack was released onto the prepatterned Au electrodes by heating the stack up to 130 °C. The PET residue was removed by dissolving in chloroform for 2 h. Finally, another few-layer graphene was added onto the top BN to work as a top gate electrode, using the top BN as the dielectric.

Magneto-PL measurements. The magneto-PL measurement was performed using a confocal micro-PL setup with the out-of-plane magnetic field. The circularly polarized excitation beam was set by a $\lambda/4$ waveplate from the linear polarized excitation laser and the laser was focused at the WSe_2 sample by a $\times 50$ objective (NA: ~ 0.65) to a spot size of ~ 2 μm . The collected PL was converted to the linear polarized light with the same $\lambda/4$ waveplate and analyzed by a CCD camera attached to a spectrograph. An assembly of a $\lambda/2$ waveplate and a second linear polarizer was used to distinguish between the $(\sigma^+\sigma^+)$ and $(\sigma^-\sigma^-)$ configurations.

Data availability

The data that support the findings of this study are available from the authors on reasonable request, see author contributions for specific data sets.

Received: 28 February 2020; Accepted: 28 May 2020;

Published online: 19 June 2020

References

- Li, Z. et al. Momentum-dark intervalley exciton in monolayer tungsten diselenide brightened via chiral phonon. *ACS Nano* **13**, 14107–14113 (2019).
- Zhu, H. et al. Observation of chiral phonons. *Science* **359**, 579–582 (2018).
- Zhang, L., Niu, Q. & Phonon V. I. Chiral phonons at high-symmetry points in monolayer hexagonal lattices. *Phys. Rev. Lett.* **115**, 115502 (2015).
- Chen, X. et al. Entanglement of single-photons and chiral phonons in atomically thin WSe_2 . *Nat. Phys.* **15**, 221–228 (2018).
- Li, Z. et al. Emerging photoluminescence from the dark-exciton phonon replica in monolayer WSe_2 . *Nat. Commun.* **10**, 2469 (2019).
- Dery, H. & Song, Y. Polarization analysis of excitons in monolayer and bilayer transition-metal dichalcogenides. *Phys. Rev. B* **92**, 125431 (2015).
- Dey, P. et al. Optical coherence in atomic-monolayer transition-metal dichalcogenides limited by electron-phonon interactions. *Phys. Rev. Lett.* **116**, 127402 (2016).
- Liu, E., Baren, J. V., Lu, Z., Taniguchi, T. & Watanabe, K. Valley-selective chiral phonon replicas of dark excitons and trions in monolayer WSe_2 . *Phys. Rev. Res.* **1**, 032007 (2019).
- Jin, C. et al. Interlayer electron–phonon coupling in WSe_2/hBN heterostructures. *Nat. Phys.* **13**, 127–131 (2017).
- You, Y. et al. Observation of biexcitons in monolayer WSe_2 . *Nat. Phys.* **11**, 477–481 (2015).
- Ye, Z. et al. Efficient generation of neutral and charged biexcitons in encapsulated WSe_2 monolayers. *Nat. Commun.* **9**, 3718 (2018).
- Chen, S.-Y., Goldstein, T., Taniguchi, T., Watanabe, K. & Yan, J. Coulomb-bound four- and five-particle intervalley states in an atomically-thin semiconductor. *Nat. Commun.* **9**, 3717 (2018).
- Li, Z. et al. Revealing the biexciton and trion-exciton complexes in BN encapsulated WSe_2 . *Nat. Commun.* **9**, 3719 (2018).
- Chow, C. M. et al. Unusual exciton-phonon interactions at van der Waals engineered interfaces. *Nano Lett.* **17**, 1194–1199 (2017).
- Wang, G. et al. Colloquium: excitons in atomically thin transition metal dichalcogenides. *Rev. Mod. Phys.* **90**, 21001 (2018).
- Novoselov, K. S., Mishchenko, A., Carvalho, A. & Castro Neto, A. H. 2D materials and van der Waals heterostructures. *Science* **353**, aac9439 (2016).
- Li, X., Zhang, F. & Niu, Q. Unconventional quantum Hall effect and tunable spin Hall effect in dirac materials: application to an isolated MoS_2 trilayer. *Phys. Rev. Lett.* **110**, 66803 (2013).
- Xu, X., Yao, W., Xiao, D. & Heinz, T. F. Spin and pseudospins in layered transition metal dichalcogenides. *Nat. Phys.* **10**, 343–350 (2014).
- Xiao, D., Yao, W. & Niu, Q. Valley-contrasting physics in graphene: magnetic moment and topological transport. *Phys. Rev. Lett.* **99**, 236809 (2007).
- Wang, Z., Shan, J. & Mak, K. F. Valley- and spin-polarized Landau levels in monolayer WSe_2 . *Nat. Nanotechnol.* **12**, 144–149 (2017).
- Rose, F., Goerbig, M. O. & Piéchon, F. Spin- and valley-dependent magneto-optical properties of MoS_2 . *Phys. Rev. B* **88**, 125438 (2013).
- Chu, R.-L. et al. Valley-splitting and valley-dependent inter-Landau-level optical transitions in monolayer MoS_2 quantum Hall systems. *Phys. Rev. B* **90**, 045427 (2014).
- Liu, G.-B., Xiao, D., Yao, Y., Xu, X. & Yao, W. Electronic structures and theoretical modelling of two-dimensional group-VIB transition metal dichalcogenides. *Chem. Soc. Rev.* **44**, 2643–2663 (2015).
- Kormányos, A. et al. k -p theory for two-dimensional transition metal dichalcogenide semiconductors. *2D Mater.* **2**, 022001 (2015).
- Krakovsky, A. & Percus, J. K. Quasiparticle effective mass for the two- and three-dimensional electron gas. *Phys. Rev. B* **53**, 7352–7356 (1996).
- Li, Z. et al. Direct observation of gate-tunable dark trions in monolayer WSe_2 . *Nano Lett.* **19**, 6886–6893 (2019).
- Zhang, X. X. et al. Magnetic brightening and control of dark excitons in monolayer WSe_2 . *Nat. Nanotechnol.* **12**, 883–888 (2017).
- Zhang, X. X., You, Y., Zhao, S. Y. F. & Heinz, T. F. Experimental evidence for dark excitons in monolayer WSe_2 . *Phys. Rev. Lett.* **115**, 257403 (2015).
- Robert, C. et al. Fine structure and lifetime of dark excitons in transition metal dichalcogenide monolayers. *Phys. Rev. B* **96**, 155423 (2017).
- Liu, E. et al. Gate tunable dark trions in monolayer WSe_2 . *Phys. Rev. Lett.* **123**, 027401 (2019).
- Zhou, Y. et al. Probing dark excitons in atomically thin semiconductors via near-field coupling to surface plasmon polaritons. *Nat. Nanotechnol.* **12**, 856–860 (2017).
- He, M. et al. Valley phonons and exciton complexes in a monolayer semiconductor. *Nat. Commun.* **11**, 618 (2020).

33. Giustino, F. Electron-phonon interactions from first principles. *Rev. Mod. Phys.* **89**, 015003 (2017).
34. Aivazian, G. et al. Magnetic control of valley pseudospin in monolayer WSe₂. *Nat. Phys.* **11**, 148–152 (2015).
35. Van Tuan, D., Scharf, B., Žutić, I. & Dery, H. Marrying excitons and plasmons in monolayer transition-metal dichalcogenides. *Phys. Rev. X* **7**, 041040 (2017).
36. Smoleński, T. et al. Interaction-induced Shubnikov–de Haas oscillations in optical conductivity of monolayer MoSe₂. *Phys. Rev. Lett.* **123**, 097403 (2019).
37. Goldberg, B. B., Heiman, D., Pinczuk, A., Pfeiffer, L. & West, K. Optical investigations of the integer and fractional quantum Hall effects: energy plateaus, intensity minima, and line splitting in band-gap emission. *Phys. Rev. Lett.* **65**, 641–644 (1990).
38. Chen, W. et al. Interaction of magnetoexcitons and two-dimensional electron gas in the quantum Hall regime. *Phys. Rev. Lett.* **64**, 2434–2437 (1990).
39. Nurmikko, A. & Pinczuk, A. Optical probes in the quantum Hall regime. *Phys. Today* **46**, 24–32 (1993).

Acknowledgements

This work is primarily supported by AFOSR through Grant FA9550-18-1-0312. T.W. and S.-F.S. acknowledge support from ACS PRF through Grant 59957-DNI10. Z. Lian and S.-F.S. acknowledge support from NYSTAR through Focus Center-NY-RPI Contract C150117. The device fabrication was supported by the Micro and Nanofabrication Clean Room (MNCR) at Rensselaer Polytechnic Institute (RPI). S.T. acknowledges support from NSF DMR-1904716, DMR-1838443, and CMMI-1933214. K.W. and T.T. acknowledge support from the Elemental Strategy Initiative conducted by the MEXT, Japan and the CREST (JPMJCR15F3), JST. Z. Lu and D.S. acknowledge support from the US Department of Energy (DE-FG02-07ER46451) for magneto-photoluminescence measurements performed at the National High Magnetic Field Laboratory, which is supported by National Science Foundation through NSF/DMR-1644779 and the State of Florida. Y.L. and C.Z. are supported by AFOSR (Grant No. FA9550-16-1-0387), NSF (Grant No. PHY-1806227), and ARO (Grant No. W911NF-17-1-0128). S.-F.S. also acknowledges the support from NSF through Grant DMR-1945420, the support from a KIP grant from RPI, and a VSP grant from NHMFL.

Author contributions

S.-F.S. conceived the experiment. Z. Li, T.W., Y.M., and Z. Lian fabricated the devices. T.W., Z. Li, S.M., Z. Lu, and Z. Lian performed the measurements. S.-F.S., T.W., S.M., Z. Li, and C.J. analyzed the data. S.-F.S., Y.L., C.J., W.Y., and C.Z. developed the theo-

retical understanding. T.T. and K.W. grew the BN crystals. S.T. and M.B. grew high-purity WSe₂ crystals through the flux zone growth technique. S.-F.S. supervised the project. D.S. supervised the magneto-PL measurements. S.-F.S. wrote the manuscript with input from all the other co-authors. All authors discussed the results and contributed to the manuscript.

Competing interests

The authors declare no competing interests.

Additional information

Supplementary information is available for this paper at <https://doi.org/10.1038/s41467-020-16934-x>.

Correspondence and requests for materials should be addressed to S.-F.S.

Peer review information *Nature Communications* thanks the anonymous reviewers for their contribution to the peer review of this work.

Reprints and permission information is available at <http://www.nature.com/reprints>

Publisher's note Springer Nature remains neutral with regard to jurisdictional claims in published maps and institutional affiliations.



Open Access This article is licensed under a Creative Commons Attribution 4.0 International License, which permits use, sharing, adaptation, distribution and reproduction in any medium or format, as long as you give appropriate credit to the original author(s) and the source, provide a link to the Creative Commons license, and indicate if changes were made. The images or other third party material in this article are included in the article's Creative Commons license, unless indicated otherwise in a credit line to the material. If material is not included in the article's Creative Commons license and your intended use is not permitted by statutory regulation or exceeds the permitted use, you will need to obtain permission directly from the copyright holder. To view a copy of this license, visit <http://creativecommons.org/licenses/by/4.0/>.

© The Author(s) 2020